Available online at www.sciencedirect.com

jmr&t Journal of Materials Research and Technology

https://www.journals.elsevier.com/journal-of-materials-research-and-technology

Original Article

Retransformation of dynamically induced ferrite during physical simulation of Steckel mill hot rolling

Thiago Bruno Carneiro[a], *Samuel Filgueiras Rodrigues*[a,*], *Clodualdo Aranas Jr.*[b], *Fulvio Siciliano*[a,c], *Eden Santos Silva*[a], *Gedeon Silva Reis*[a], *Edson Jansen Pedrosa Miranda Jr.*[a], *Valdemar Silva Leal*[a], *Mohammad Jahazi*[d], *John Joseph Jonas*[e]

[a] *Graduate Program in Materials Engineering, Federal Institute of Education, Science and Technology of Maranhão, Sao Luis 65075-441, Brazil*

[b] *Mechanical Engineering, University of New Brunswick, Fredericton, NB E3B 5A3, Canada*

[c] *Dynamic Systems Inc. 323 NY 355, Poestenkill, New York 12140, US*

[d] *Department of Mechanical Engineering, Ecole de Technologie Supérieure, H3C 1K3, Montreal, Canada*

[e] *Department of Materials Engineering, McGill University, H3A 0C5, Montreal, Canada*

ARTICLE INFO

Article history:
Received 9 June 2020
Accepted 13 July 2020
Available online 27 July 2020

Keywords:
Dynamic transformation
Strain-induced ferrite
Steckel mill hot rolling

ABSTRACT

It has been well established that austenite can partially transform into ferrite during thermomechanical processing. The laboratory-scale strip and plate rolling simulations in the literature suggest that both forward and backward dynamic transformation (DT) can occur above the equilibrium Ae_3 temperature. In this work, a five-pass Steckel mill rolling schedule (isothermal deformation) of an X70 high Nb steel was simulated using a torsion testing machine. Four different roughing schedules with a strain of 0.4 per pass were employed at 1100 °C before the application of finishing passes. A total of five finishing passes were simulated at 900 °C with pass strains of 0.3, strain rate of 1.0 s^{-1}, and interpass time of 10 s, followed by isothermal holding varying from 1 to 270 s. The level of the flow curves depicted activation of softening phenomena, which was shown to be the formation of DT ferrite by means of optical and scanning electron microscopy images. The volume fraction of DT ferrite increases with increasing the number of roughing passes due to retained work hardening. Moreover, the DT ferrite retransforms back into austenite during the 10 s pass interval and holding after last strains, as shown by phase fraction measurement before and after each pass. Thus, the interpass time and holding intervals after the simulations play a significant role in reducing the amount of ferrite after the process. It seems that the presence

* *Corresponding author.*
E-mail: samuel.filgueiras@ifma.edu.br (S.F. Rodrigues).

https://doi.org/10.1016/j.jmrt.2020.07.042

of Nb in the alloy affects both the forward and backward transformation. The present investigation can be used to estimate the amount of formed and retransformed ferrite during Steckel mill operations in order to have a better metallurgical understanding of the process. This may result in better dimensional and quality control during the manufacturing of X70 pipeline steels.

1. Introduction

High strength low alloy steels (HSLA) present excellent mechanical properties such as very high toughness and strength over a wide temperature range, good weldability, and exceptional crack arrestability [1–3]. These materials have been used as linepipe steels to respond the increasing demand for oil and gas transportation around the world and complexity of these operation systems [4]. Sophisticated designs and well planned projects to improve or even develop higher grades of these materials are required before making them available to operate under severe conditions like high pressures and loads [5]. These steels are produced through hot rolling and undergo a series of thermomechanical control processing (TMCP) at high temperatures. During the TMCP, the microstructure undergoes several cycles of hardening followed by dynamic and static softening stages, such as dynamic recrystallization (DRX) and dynamic recovery (DRV) [6]. In addition to these phenomena, dynamic transformation (DT) of austenite to ferrite [7–11] plays an important role during hot deformation and affects the final microstructure of the material.

Recently, by means of in-situ X-ray diffraction experiments [12–14], the DT has been proved to take place during the hot deformation of a large family of steels above the Ae_3 temperature. The formation of ferrite can be dynamically induced at elevated temperatures due to the added free energy to the austenite phase, either from the applied stress [14] or high dislocation density [16], which makes the austenite phase less stable. Note that the occurrence of DT primarily depends on the chemical composition of the steel, temperature, and percent deformation. Its transformation mechanism can be either displacive, diffusional, or a combination of displacive and diffusional, which remains to be confirmed. This unusual metallurgical phenomenon was also observed in titanium and zirconium alloys [17–20]. Most of the time, a hard phase dynamically transforms into a softer phase.

Since ferrite is softer than austenite, phase transformation softens the material during deformation and can affect the thermomechanical processing of steels [21]. This softening phenomenon affects the selection of the TMCP parameters. Specifically, it could affect the rolling force during deformation and may lead to shape control issues. Although various models have been developed to account for DRX and DRV during thermomechanical processing, the studies related to the DT are limited [7–16,22–26]. To date, most of the DT studies are related to plate and strip rolling (i.e., continuous cooling condition) [27–29]. In these studies, it has been established that although austenite transforms into ferrite during hot deformation, retransformation occurs during the intervals from one rolling mill to another. Due to unloading, the dynamically transformed ferrite retransforms back to austenite which is more thermodynamically stable above Ae_3. The kinetics of the forward and backward transformations were quantified by measuring the volume fraction of ferrite from one pass to another. However, despite the recent progress in this area, a quantitative analysis related to the formation and retransformation of ferrite during the Steckel mill hot rolling process [30] has not been studied in more detail yet.

In the present work, multi-deformation schedules are applied isothermally rather than during cooling. A five-pass Steckel mill rolling was physically simulated using a torsion testing machine, and dynamically formed, and retransformed ferrite were quantified. The results can be used to assess and estimate the amount of DT ferrite after each pass during the hot rolling of a X70 steel grade for more control of the manufacturing process and mechanical properties of the final product.

2. Material and methods

A hot-rolled Nb-microalloyed X70 steel plate was utilized in this work. The chemical composition showing the main elements of the alloy is presented in Table 1. The Ae_3 temperatures were calculated using the JMatPro v12 thermodynamic simulation software employing the General Steel module. Torsion samples, with diameters of 6.4 mm and gage lengths of 22.2 mm, were machined from the as received plates. Here the length of the torsion sample is parallel to the rolling direction. Hot torsion tests were carried out using the MTS torsion machine equipped with a radiation furnace and temperature controller. All the experiments were conducted under an argon gas atmosphere. The torque-twist data from the torsion machine was converted into equivalent stress-strain curves using the Fields and Backofen equations [31].

The thermomechanical schedule of the Steckel mill rolling simulation is displayed in Fig. 1. The samples were initially heated to the austenitization temperature of 1200 °C at a rate of 1 °C/s. The temperature was held for 20 min, followed by cooling to a roughing pass temperature of 1100 °C. Roughing schedule was then applied with pass strain and strain rate of 0.4 and 1 s^{-1}, respectively. Four different roughing thermomechanical schedules were employed: i) zero pass, ii) one pass, ii) two passes, and iv) three passes. After the rouging process, the samples were cooled to 900 °C followed by a five-pass isothermal finishing passes with pass strain, strain rate and interpass time of 0.3, 1 s^{-1}, and 10 s, respectively. Five isothermal holding times were employed after multi-pass deformation: i) 1 s, ii) 10 s, iii) 30 s, iv) 90 s, and v) 270 s. All the samples were

Table 1 – Chemical composition (wt%) and equilibrium transformation temperatures (°C).

C	Mn	Si	Cr	Nb	N	Orthoequilibrium Ae_3	Paraequilibrium Ae_3
0.047	1.56	0.25	0.21	0.092	0.008	845 °C	810 °C

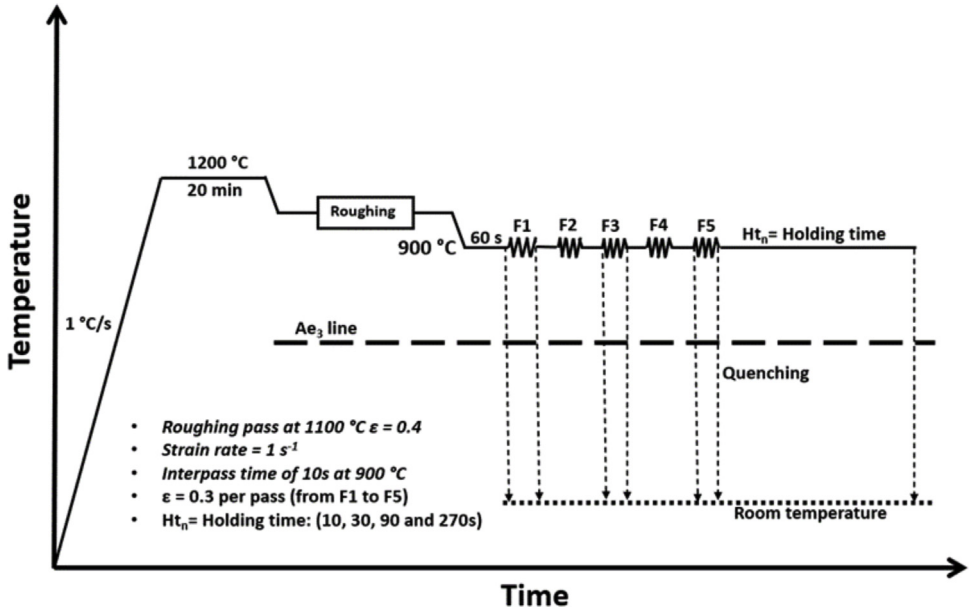

Fig. 1 – Thermomechanical schedule of the laboratory-scale torsion simulation of Steckel mill rolling operation.

water quenched after the following conditions: i) before the first finishing pass, ii) after the first pass, iii) before the third pass, iv) after the third pass, v) before the fifth pass, and vi) after the fifth pass. This approach allows for the measurement of dynamically transformed and retransformed ferrite during deformation and pass intervals.

The microstructures were obtained from 150 μm below the surface of the specimens to avoid any external surface effect. The quenched samples were rough polished using SiC paper from 400 to 1200 grit, followed by diamond suspension fine polishing from 3 μm to 1 μm and 0.02 μm colloidal silica suspension. The etching was done using a 3% Nital and 10% aqueous sodium metabisulfite solution ($Na_2S_2O_5$) solution in order to improve the contrast between ferrite and martensite. The microstructures were analyzed using optical and electron microscopy (Hitachi SU8230 at an accelerating voltage of 15 kV) imaging. An Energy Dispersive X-ray Spectroscopy (EDS) analysis was performed to verify the presence of precipitates. For the microhardness measurement, a Clemex CMT microhardness Vickers tester was used following the standard ASTM E92.

3. Results and discussion

3.1. *Stress-strain curves*

The flow curves after no roughing, one, two and three roughing passes are displayed in Fig. 2a, 2b, 2c, and 2d, respectively. For all testing conditions, the stress magnitude from first to the second finishing pass significantly increases by 18.5% (Fig. 2a), 17.9% (Fig. 2b), 16.8% (Fig. 2c), and 13.5% (Fig. 2d). This stress increase is due to strain accumulation, which increases the dislocation density of the material. The rate of increase appears to be the lowest in the sample with three roughing passes, see Fig. 2d. The increase in stress in the second pass is followed by a gradual decrease from the second pass until the fifth and final pass. The rate of decrease is highest in the 3-roughing pass condition (5 MPa per pass) as illustrated in Fig. 2d.

In hot rolling, mean flow stress (MFS) provides a good indication whether a softening or hardening metallurgical phenomena take place such as work hardening, recrystallization, recovery, and phase transformations [32]. MFS depends on deformation temperature, strain, and strain rate, and can be obtained by integrating a stress-strain curve normalized by the amount of strain. In the present work, the MFS's were calculated from the stress-strain curves of Fig. 2 and are presented in Fig. 3. The samples tested with zero, one, two and three roughing passes are displayed in different curves. The MFS's after the first pass are similar to all other conditions, although a slightly lower MFS can be seen for the condition with the most number of roughing passes. This indicates that prior softening phenomena took place during roughing passes, such as dynamic and static recrystallization and recovery. Then, from the first to the second pass, a drastic increase of MFS by 43.1% (no roughing), 39.9% (one roughing), 37.9% (two roughing), and 35.3% (three roughing) can be seen. There is a slight MFS increase between the second and the third pass. However, from the third pass until the fifth and final pass, the MFS's decreased by 3.5% (no roughing pass), 5.4% (one roughing pass), 6.7% (two roughing passes), and 11.3%

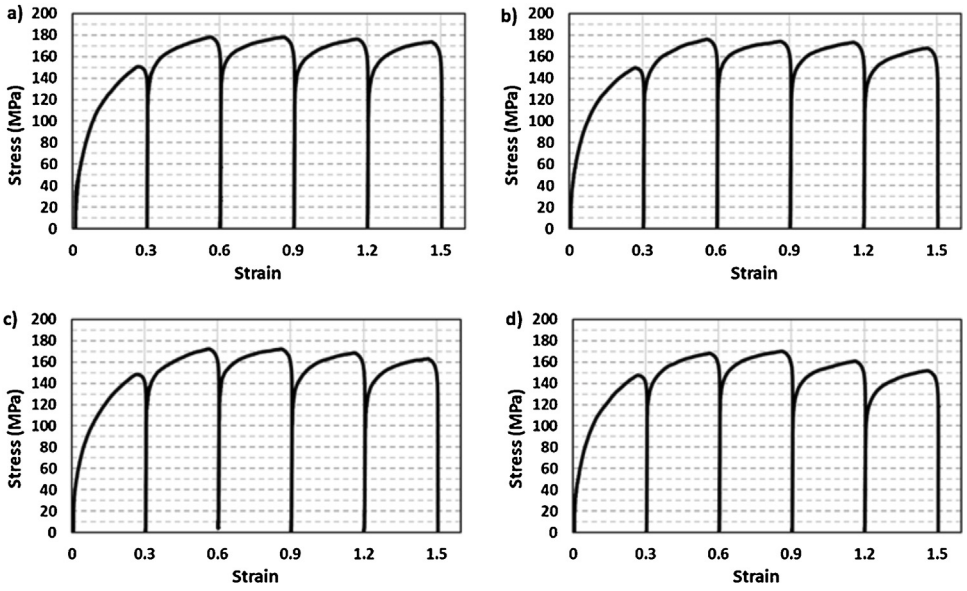

Fig. 2 – Stress-strain curves obtained from torsion simulation of the finishing rolling schedule with a) no roughing, b) one roughing pass, c) two roughing passes, and d) three roughing passes.

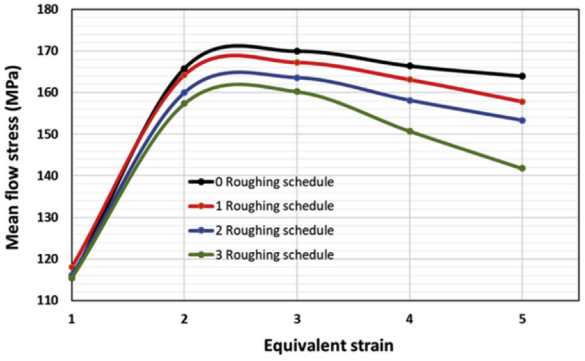

Fig. 3 – Calculated mean flow stresses (MFS) from the stress-strain curves in Fig. 2. A systematic decrease in MFS can be seen from third until the fifth and final pass.

(three roughing passes). Based on the above findings could be said that the number of roughing affects the stresses during the simulation, and this may be reflected in the roll forces. This will be analyzed further in the following sections.

3.2. *Optical microstructural analysis*

The optical microstructures before the first pass for all the testing conditions were taken and are presented in Fig. 4. The sodium metabisulfite etchant provides a contrast between the phases based on dislocation density. Thus, the freshly formed ferrite (lighter regions) can be separated from martensite with high dislocation density (prior austenite at elevated temperature). Figs. 4a, 4b, 4c, and 4d depict the microstructures with zero, one, two, and three number of roughing passes, respectively. More notably, the sample with no roughing passes displays a completely martensitic structure. On the other hand, the samples with roughing passes have minor amounts of ferrite. Based on the analysis of the quenched samples, the formation of ferrite in these samples could be related to roughing passes: however, the trend in the amount of ferrite is not so obvious.

The microstructures of the samples before the third finishing pass with different roughing schedules are presented in Fig. 5**a** (no roughing pass), **5b** (one roughing pass), **5c** (two roughing passes) and **5d** (three roughing passes). In Fig. 5a, although the microstructure is mostly martensitic, there are minor traces of ferrite (bright regions). These results reveal that deformation above the Ae_3 induced the formation of ferrite; however, it must be noted that the microstructures in Fig. 5 was obtained 10 s after the 2nd deformation (finishing pass). This delay allows the retransformation of dynamically transformed ferrite [29]; therefore, only traces of ferrite were detected. On the other hand, for samples with one (Fig. 5b), two (Fig. 5c), and three (Fig. 5d) roughing passes, the presence of ferrite can be clearly seen from the samples. It appears that more ferrite was formed for the tests with a higher number of roughing passes.

Finally, in Fig. 6, the microstructures of samples before the fifth and final pass are shown. Similar to Fig. 5, only traces of ferrite are evident in Fig. 6a (no roughing pass). On the other hand, for samples with one (Fig. 6b), two (Fig. 6c) and three (Fig. 6c) roughing passes, more ferrite can be detected on samples with a higher number of roughing passes.

3.3. *Volume fraction of ferrite*

The stress-strain curves in Fig. 2 display a significant drop in stress. The softening could be related to the occurrence of both DT and DRX, as illustrated in the literature [33,34]. Based on the optical microstructures, a softer ferrite phase was formed, and retransformed back into austenite (shown here as martensite due to water quenching). For quantitative analysis, the volume fraction of ferrite was measured for each

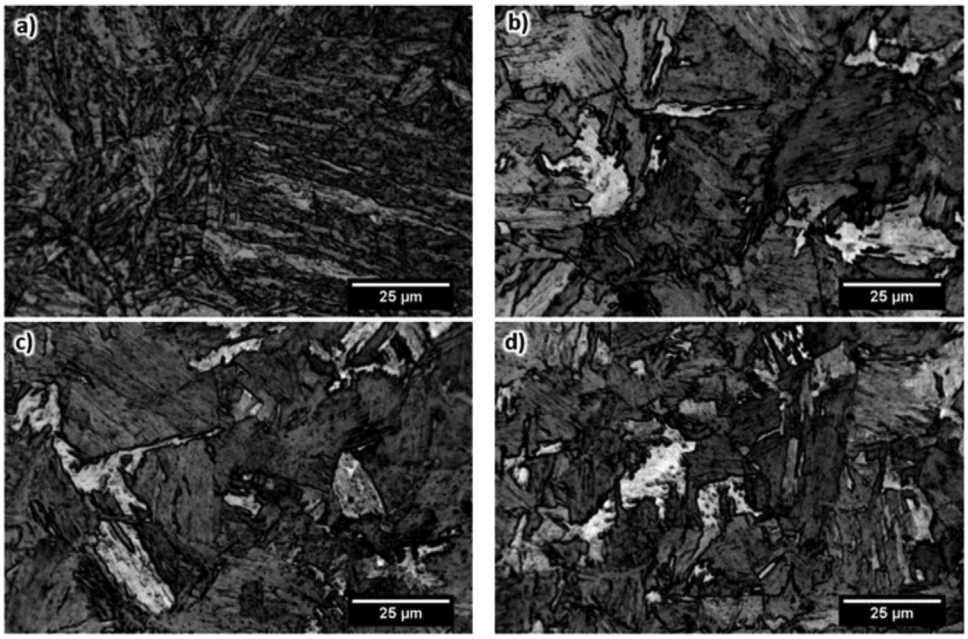

Fig. 4 – Optical micrographs of the samples before the first pass. a) no roughing, b) one roughing pass, c) two roughing passes, and d) three roughing passes.

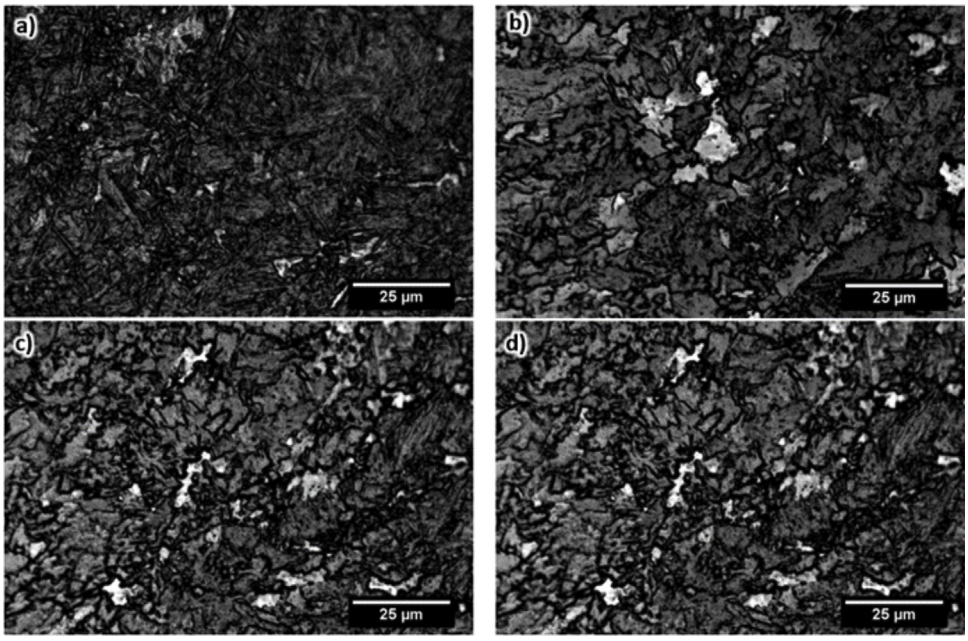

Fig. 5 – Optical micrographs of the sample before the third pass. a) no roughing, b) one roughing pass, c) two roughing passes, and d) three roughing passes.

condition, as displayed in Fig. 7. Each figure is divided into two parts: i) cumulative ferrite right after each pass, and ii) cumulative ferrite before each pass. This approach will determine the amount of ferrite that disappeared as a result of reverse transformation.

In Fig. 7a (associated with the sample with no roughing pass), the volume fraction of ferrite after the 1 st pass is 4.4%. This amount increases to 10.0% percent after the 3rd pass and generates a total of 20.5% of ferrite after the last pass. In order to provide a better understanding of what happens during the 10 s interpass time, the volume fraction of ferrite was measured before each pass. The difference between the fraction of ferrite before and after each pass provides the amount of DT ferrite that formed during deformation, as well as the amount of ferrite disappeared within 10 s interval as a result of diffusional retransformation [25]. Before the finishing passes, there is no ferrite observed as supported by optical microstructures above. Then, before the 3rd and 5th passes, the volume

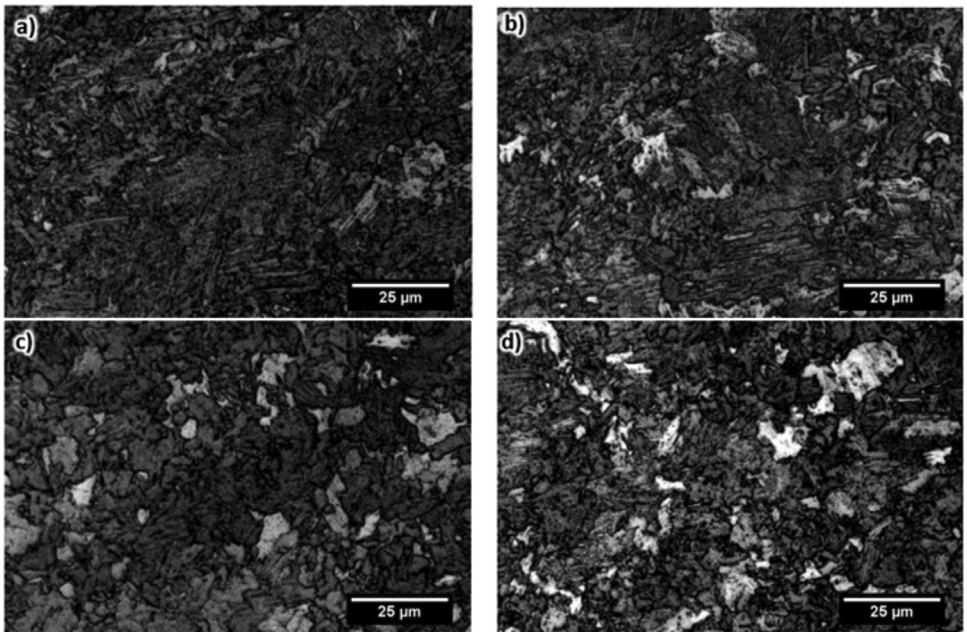

Fig. 6 – Optical micrographs of the sample before the fifth pass. a) no roughing, b) one roughing pass, c) two roughing passes, and d) three roughing passes.

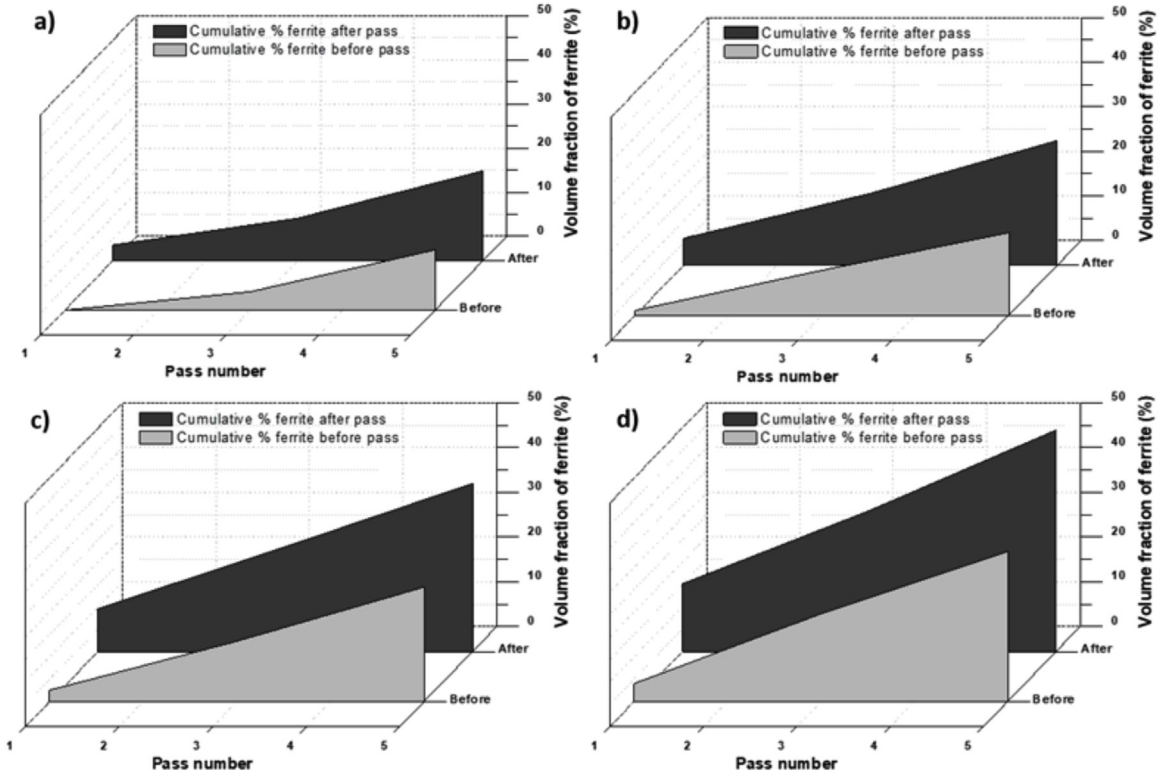

Fig. 7 – Measured volume fraction of ferrite before and after each pass. a) no roughing, b) one roughing pass, c) two roughing passes, and d) three roughing passes.

fractions of ferrite were measured at 4.8% and 13.8%, respectively. Note that the 13.8% DT ferrite volume fraction (before the 5th pass), increased to 20.5% (immediately after the 5th pass), which means the 5th pass alone provided a total of 6.7% ferrite. Similarly, this information allows for quantification of DT ferrite that retransformed during the 10 s interpass time. For example, 15.1% volume fraction of DT ferrite was formed after the 4th pass; however, 13.8% was measured before the

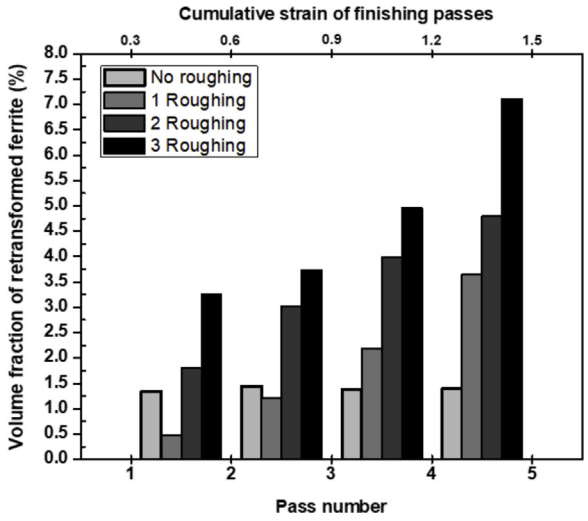

Fig. 8 – Calculated amount of ferrite that retransformed during the interpass interval.

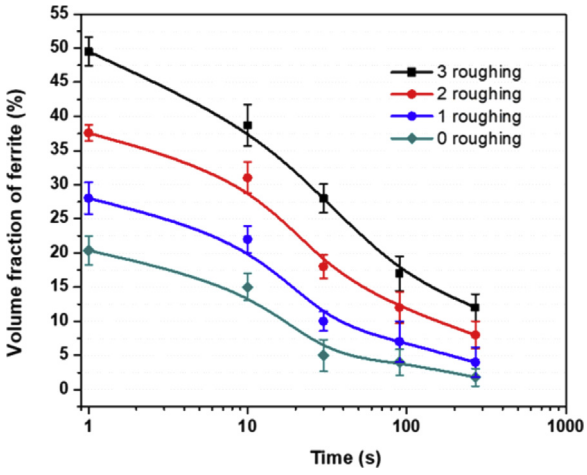

Fig. 10 – The measured volume fraction of ferrite during isothermal holding to track the reverse transformation of DT ferrite into austenite.

5th pass. This means that during 10 s interval between the 4th and 5th pass, 1.3% of ferrite reverted into austenite. This approach was utilized later to quantify the amount of ferrite formed and retransformed after each pass.

For the sample with one roughing pass (see Fig. 7b), the volume fraction of ferrite after the 1 st, 3rd, and 5th passes were 6.3%, 16.6%, and 28.0%, respectively. On the other hand, before the 1 st, 3rd, and 5th passes, the amounts of ferrite were 1.0%, 10.1%, and 18.5%, respectively. Similarly, the results for the two-roughing pass simulation (see Fig. 7c) has volume fractions of 9.6% (after the 1 st pass), 23.4% (after the 3rd pass), and 38% (after the 5th pass). These volume fractions are lower before the 1 st (2.9%), 3rd (13.4%), and 5th (25.9%) passes. Finally, for simulation with three roughing passes in Fig. 7d, the volume fractions after each pass were 15.1% (1 st pass), 31.9% (3rd pass), and 49.8% (5th pass). On the other hand, these numbers were lower before each pass, 4.1% (1 st pass), 19.2% (3rd pass), and 33.5% (5th pass).

Generally, higher fractions of DT ferrite were detected for testing conditions with higher number of roughing passes. The prior strains before finishing passes generated DT ferrite, and the ferrite may retransform during cooling to the finishing pass temperature [11]. Note that all the temperatures employed are above the Ae_3; thus, no phase transformation is expected during the process. However, significant phase transformation was detected in every step of the simulation. In this work, it is evident that DT ferrite was formed dynamically, and may retransform back into austenite upon isothermal holding at temperatures above the Ae_3.

The numbers in Fig. 7 were employed to generate the total fraction of ferrite that retransformed into austenite during the 10 s interpass time, as displayed in Fig. 8. The values were calculated by subtracting the volume fraction of ferrite after a certain pass number from the amount measured before the next pass. During the initial stages of the Steckel mill rolling simulation, the volume fraction of ferrite that retransformed is lower compared to that of the later stages. This is due to the cumulative interpass time in the whole process, which allows for a higher amount of reverse transformation of ferrite, as much as 7.1% for the three-roughing pass simulation. The simulation with absence of roughing passes only registered 1.4% of retransformed ferrite. The results in this figure can be used to properly account for the retransformation rate in between passes based on the number of roughing passes. It can be seen here that the no-roughing pass test has a relatively low amount or reverse transformation as compared to

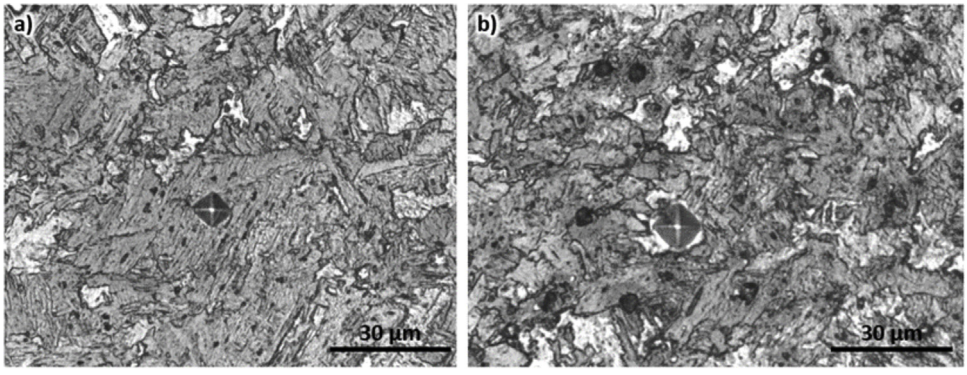

Fig. 9 – Microhardness measurement performed on individual grains to verify the existence of ferrite and martensite in the microstructure.

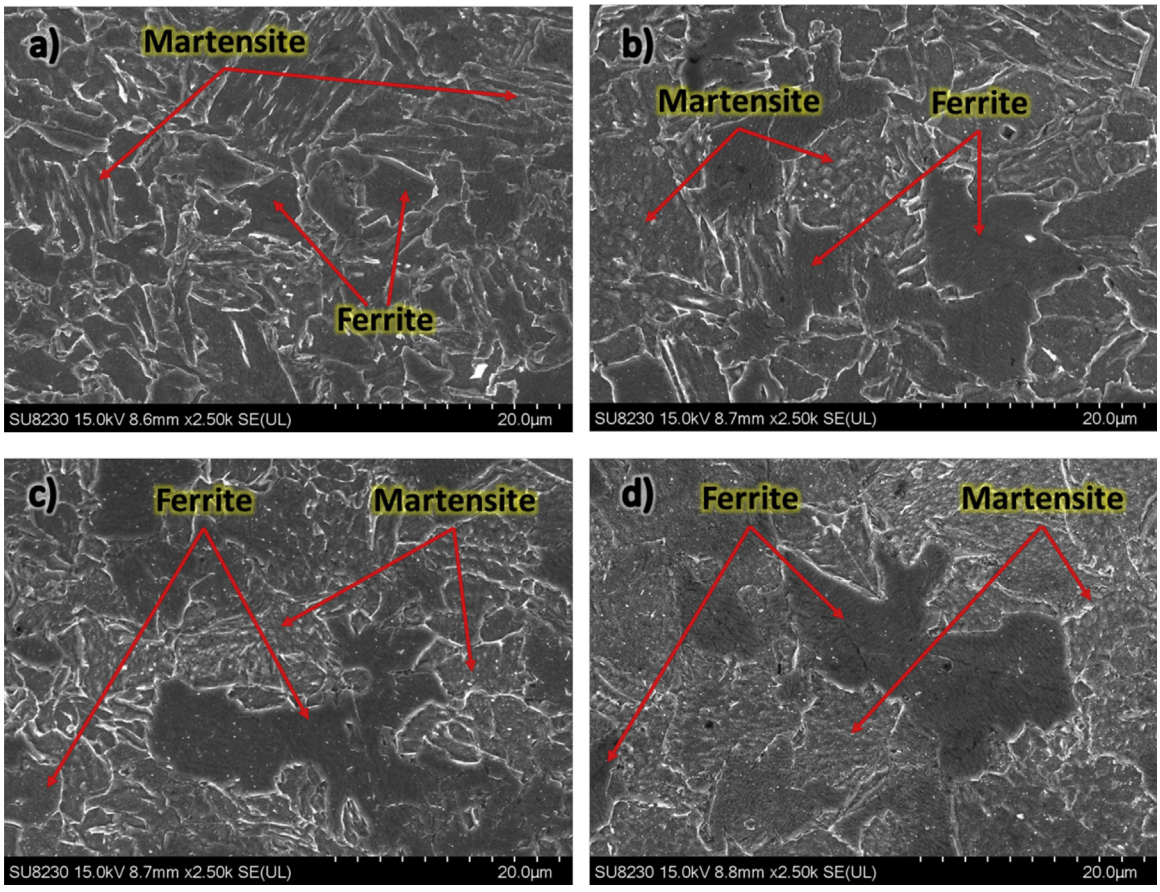

Fig. 11 – Scanning electron microscopy images of the samples after isothermal holding of a) 10 s with three roughing passes, b) 270 s with three roughing passes, c) 10 s with no roughing pass, and d) 270 s with no roughing passes.

the simulation with one or more roughing passes. It is also important to note that one of the reasons for this observation is the higher fraction of ferrite formed in simulations with roughing passes; thus, it allows more volume fraction of ferrite to retransform back into austenite phase.

The presence of both ferrite and martensite phases were confirmed by microhardness measurements to verify the validity of the volume fractions above, as displayed in Fig. 9. It can be seen that the dark region has a smaller indentation print with an average value of 354 HV (see Fig. 9a) and the lighter region has an average hardness of 183 HV (see Fig. 9b). This result supports the idea that the dark areas are martensite, whereas the lighter areas are ferrite.

3.4. *Retransformation of DT ferrite after isothermal holding*

The effect of isothermal holding times on the final microstructure (after the Steckel mill simulation) was also investigated. Although it is well-known that isothermal holding initiates the reverse DT process [29], the chemical composition is an essential factor in modeling the rate of diffusional retransformation of DT ferrite [15,16,35]. The present material is X70 pipeline steel with an amount of niobium higher than usual. This alloying element is known to delay the retransformation process by means of solute drag and/or precipitate pinning effect [8]. Without the niobium effect, it may be possible to retransform the DT ferrite completely back into austenite within tens of seconds [9,25,33]. To further analyze the retransformation of X70 after Steckel mill hot rolling, the volume fraction of ferrite was tracked during isothermal holding, and the results are presented in Fig. 10. The volume fractions of ferrite after the simulation are 20.6%, 28.3%, 37.8%, and 49.8%, respectively, for zero, one, two, and three roughing passes. The values decrease to 15.1% (no roughing pass), 22.1% (one roughing pass), 31.0% (two roughing passes), and 38.9% (three roughing passes) after 10 s of isothermal holding. These values further decrease after 30 s and 90 s of isothermal holding. Finally, the amounts of ferrite after 270 s of holding are 1.9%, 2.4%, 8.0%, and 12.1% for zero, one, two, and three roughing passes, respectively. It can be seen here that the simulation with the highest number of roughing passes requires longer holding time to completely transform the metastable DT ferrite back into austenite. In the present experimental conditions, it may be required up to 1000s (or more) for the three-roughing pass simulation to retransform all the DT ferrite formed in the simulation. As mentioned above, the retransformation rate of the present alloy is quite slow compared to plain-C steel [23,29,35,36] due to the presence of Nb in the alloy.

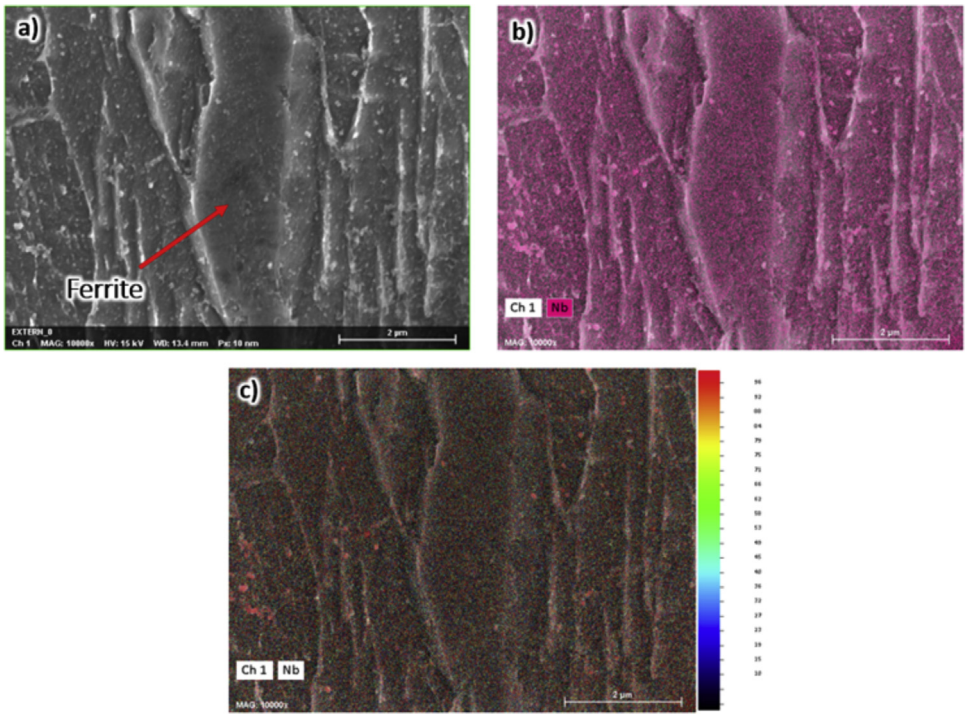

Fig. 12 – Energy Dispersive X-ray Spectrophotometry (EDS) analysis of the sample after finishing passes with no roughing pass and 10 s holding.

3.5. *Scanning electron microscope (SEM) examination of the microstructure*

SEM microstructures of some specimens sectioned transversely after the finishing stage of the torsion simulation, that is, during holding are presented in Fig. 11. These were taken in order to qualitatively evaluate the retransformation behavior of the ferrite into austenite. Ferrite is mostly present in the polygonal form. These are highlighted by arrows in sample images with different thermomechanical schedules, 10 s holding with three roughing passes (see Fig. 11a), 270 s holding with three roughing passes (see Fig. 11b), 10 s holding with no roughing passes (see Fig. 11c) and 270 s holding with no roughing passes (see Fig. 11d). It is clear that the amount of ferrite presented during holding was affected by the applied strain, include roughing, along the simulation. Higher amount of ferrite was observed in Fig. 11a than in Fig. 11c and a similar trend is observed between Fig. 11b and Fig. 11d. The polygonal ferrites zones are bigger for the schedule with no roughing and longer holding time due to less accumulated strain and more time for diffusional coalescence and growth, respectively [29].

An EDS analysis was performed to verify the presence of Nb precipitates that may have pinned the movement of grain boundaries during the diffusional re-transformation of DT ferrite back into austenite, as displayed in Fig. 12. This sample was taken from the tests without any roughing pass and 10 s holding. In Fig. 12a, ferrite plates are evident, which are known to have near-identical crystallographic orientation and are self-accommodating plates [10,37]. These features allow for the formation of polygonal grains upon continued straining [8,27]. The maps in Fig. 12b and 12c reveal the existence of niobium precipitates. These precipitates are near the vicinity of the grain boundaries; thus, delaying the retransformation process, which may require more than 1000s if the process implements a multi-pass roughing strain.

4. Conclusions

In this work, dynamic forward and reverse transformations of ferrite during Steckel mill hot rolling simulation of a X70 steel were presented. Based on the experimental results, the following conclusions can be drawn:

1 The softening detected in the stress-strain curves is related to the formation of DT ferrite as shown in the microstructures observed by optical microscopy. The presence of both ferrite and martensite was supported by the hardness measurement of individual grains.
2 The increase in the number of roughing passes affects the amount of DT ferrite during the Steckel mill hot rolling process. The addition of a three-roughing pass schedule resulted in up to 50% of DT ferrite. This amount of DT ferrite needs more than 1000s of isothermal holding (after the final deformation) to completely retransform the DT ferrite phase into austenite.
3 The retransformation of DT ferrite was affected by the number of roughing passes. It was shown that only less than 2% of DT ferrite was retransformed after each interpass interval for the simulation without a roughing pass. For tests with three roughing passes, an average of 5% of DT ferrite is retransformed during the interpass interval in Steckel mill hot rolling simulation.

4 The presence of Nb in the alloys delayed the diffusional retransformation of DT ferrite into austenite. For the present material, Nb rich precipitates were detected, which can pin the grain boundaries of DT ferrite and delay the diffusional phase transformation from ferrite to austenite.

Conflicts of interest

The authors declare no conflicts of interest.

Acknowledgments

The authors are grateful for the financial support from the Brazilian National Council for Scientific and Technological Development (CNPq), Research and Support Foundation of Maranhão (FAPEMA), Natural Sciences and Engineering Research Council of Canada (NSERC), New Brunswick Innovation Foundation (NBIF) and Harrison McCain Foundation.

REFERENCES

[1] Liu L, Xiao H, Li Q, Liu Y, Li P, Yang Z, et al. Evaluation of the fracture toughness of X70 pipeline steel with ferrite-bainite microstructure. Mater Sci Eng A 2017;688:388–96 https://doi.org/10.1016/j.msea.2017.01.043.

[2] Moraes CAP, Chludzinski M, Nunes RM, Lemos GVB, Reguly A. Residual stress evaluation in API 5L X65 girth welded pipes joined by friction welding and gas tungsten arc welding. J Mater Res Tech 2019;8(1):988–95 https://doi.org/10.1016/j.jmrt.2018.07.009.

[3] Pumpyanskyi DA, Lobanova TP, Pyshmintsev IY, Arabey AB, Stolyarov VI, Kharionovsky VV, et al. Crack propagation and arrest in X70 1420x21,6mm pipes for new generation of gas transportation system. 7th International Pipeline Conference; 2008. IPC2008-64474:365-370, https://doi.org/10.1115/IPC2008-64474.

[4] Shahrani A, Yazdipour N, Ali D, Grazder A, Cayron C, Pereloma E. The effect of processing parameters on the dynamic recrystallization behavior of API-X70 pipeline steel. Mater Sci Eng A 2013;570:70–81 https://doi.org/10.1016/j.msea.2013.01.066.

[5] Yoo JY, Ahn SS, Seo DH, Song WH, Kang KB. New development of high grade X80 to X120 pipeline steels. Mater Man Proc 2011;26(1):154–60 https://doi.org/10.1080/10426910903202534.

[6] Sakai T, Belyakov A, Kaibyshev R, Miura H, Jonas JJ. Dynamic and post-dynamic recrystallization under hot, cold and severe plastic deformation conditions. Prog Mater Sci 2014;60:130–207 https://doi.org/10.1016/j.pmatsci.2013.09.002.

[7] Zhao L, Park N, Tian Y, Shibata A, Tsuji N. Dynamic transformation mechanism for producing ultrafine grained steels. Adv Eng Mater 2018;20:1701016 https://doi.org/10.1002/adem.201701016.

[8] Ghosh C, Aranas C, Jonas JJ. Dynamic transformation of deformed austenite at temperatures above the Ae_3. Prog Mater Sci 2016;82:151–233 https://doi.org/10.1016/j.pmatsci.2016.04.004.

[9] Aranas C, Shen Y, Rodrigues SF, Jonas JJ. Microstructural evolution of a C-Mn steel during hot compression above the Ae_3. Metall Mater Tran A 2016;47(9):4357–61 https://doi.org/10.1007/s11661-016-3655-8.

[10] Grewal R, Aranas C, Chadha K, Shahriari D, Jahazi M, Jonas JJ. Formation of Widmastatten ferrite at very high temperatures in the austenite phase field. Acta Mater 2016;109:23–31 https://doi.org/10.1016/j.actamat.2016.02.062.

[11] Rodrigues SF, Siciliano F, Aranas C, Silva ES, Reis GS, Jahazi M, et al. Dynamic phase transformation behavior of a Nb-microalloyed steel during roughing passes at temperatures above the Ae_3. Metals 2019;9(3):334 https://doi.org/10.3390/met9030334.

[12] Yada H, Li C-M, Yamagata H. Dynamic $\gamma \rightarrow \alpha$ Transformation during hot deformation in iron–nickel–carbon alloys. ISIJ Inter 2000;40(2):200–6 https://doi.org/10.2355/isijinternational.40.200.

[13] Shibata A, Takeda Y, Park N, Zhao L, Harjo S, Kawasaki T, et al. Nature of dynamic ferrite transformation revealed by in-situ neutron diffraction analysis during thermomechanical processing. Scripta Mater 2019;165:44–9 https://doi.org/10.1016/j.scriptamat.2019.02.017.

[14] Aranas C, Rodrigues SF, Siciliano F, Jonas JJ. In-situ X-ray diffraction evidence of dynamic transformation of austenite to ferrite during hot compression test in the single austenite phase field. Scripta Mater 2020;177:86–90 https://doi.org/10.1016/j.scriptamat.2019.10.008.

[15] Aranas C, Jonas JJ. Effect of Mn and Si on dynamic transformation of austenite above the Ae3 temperature. Acta Mater 2015;82:1–10 https://doi.org/10.1016/j.actamat.2014.08.060.

[16] Ghosh C, Basabe VV, Jonas JJ. Thermodynamics of dynamic transformation of hot deformed austenite in four steels of increasing carbon contents. Mater Sci Eng A 2014;591:173–82 https://doi.org/10.1016/j.msea.2013.10.077.

[17] Guo B, Aranas C, Foul A, Ji X, Fall A, Jahazi M, et al. Effect of multipass deformation at elevated temperatures on the flow behavior and microstructural evolution in Ti-6Al-4V. Mater Sci Eng A 2018;729:119–24 https://doi.org/10.1016/j.msea.2018.05.058.

[18] Foul A, Aranas C, Guo B, Jonas JJ. Dynamic transformation of $\alpha \rightarrow \beta$ titanium at temperatures below the β-transus in commercially pure titanium. Mater Sci Eng A 2018;722:156–9 https://doi.org/10.1016/j.msea.2018.02.097.

[19] Guo B, Semiatin SL, Jonas JJ, Yue S. Dynamic transformation of Ti–6Al–4V during torsion in the two-phase region. J Mater Sci 2018;53:9305–15 https://doi.org/10.1007/s10853-018-2237-0.

[20] Aranas C, Guo B, Rodrigues S, Choi J, Kim S, Sun B, et al. Deformation-induced phase transformation in Zircaloy-4 below the beta transus. Mat Let 2018;220:229–33 https://doi.org/10.1016/j.matlet.2018.03.033.

[21] Siciliano F, Rodrigues SF, Aranas C, Jonas JJ. The dynamic transformation of ferrite above the Ae_3 and the consequences on hot rolling of steels. Tecnol Metal Mater Miner 2020 https://doi.org/10.4322/2176-1523.20202230.

[22] Liu Z, Li D, Lu S, Qiao G. Thermal stability of high temperature deformation induced ferrite in a low carbon steel. ISIJ Int 2007;47:289–93 https://doi.org/10.2355/isijinternational.47.289.

[23] Basabe VV, Jonas JJ. The ferrite transformation in hot deformed 0.036% Nb austenite at temperature above the Ae_3. ISIJ Int 2010;50:1185–92 https://doi.org/10.2355/isijinternational.50.1185.

[24] Rodrigues SF, Aranas C, Wang T, Jonas JJ. Dynamic transformation of an X70 steel under plate rolling conditions. ISIJ Int 2017;57:162–9 https://doi.org/10.2355/isijinternational.ISIJINT-2016-439.

[25] Aranas C, Rodrigues SF, Shen Y-J, Zhang Z, Jonas JJ. Time-Temperature-Reverse Transformation (TTRT) behaviors of a C-Mn and a Nb microalloyed steel after dynamic transformation above the Ae_3. Steel Res Int 2017;87:1700006 https://doi.org/10.1002/srin.201700006.

[26] Rodrigues SF, Aranas C, Sun B, Siciliano F, Yue S, Jonas JJ. Effect of grain size and residual strain on the dynamic transformation of austenite under plate rolling conditions. Steel Res Int 2018;89:1700547 https://doi.org/10.1002/srin.201700547.
[27] Rodrigues SF, Aranas C, Siciliano F, Jonas JJ. Dynamic transformation during the simulation of plate rolling in an X70 Steel. Steel Res Int 2016;87:1600388 https://doi.org/10.1002/srin.201600388.
[28] Rodrigues SF, Aranas C, Jonas JJ. Dynamic transformation during the simulated plate rolling of a 0.09% Nb steel. ISIJ Int 2017;57:1102–11 https://doi.org/10.2355/isijinternational.ISIJINT-2016-678.
[29] Rodrigues SF, Aranas C, Jonas JJ. Retransformation behavior of dynamically transformed ferrite during the simulated plate rolling of a low C and an X70 Nb steel. ISIJ Int 2017;57:929–36 https://doi.org/10.2355/isijinternational.ISIJINT-2016-692.
[30] Palhano HB, Aranas C, Rodrigues SF, Silva ES, Reis GS, Miranda EJP, et al. Strain-induced ferrite formation during Steckel mill simulations with varying roughing pass schedules. Metals 2019;9(8):814 https://doi.org/10.3390/met9080814.
[31] Fields DS, Backofen WA. Determination of strain hardening characteristics by torsion testing. Proc Am Soc Test Mater 1957;57:1259–72.
[32] Siciliano F, Jonas JJ. Mathematical modeling of the hot strip rolling of microalloyed Nb, multiply-alloyed Cr-Mo, and plain C-Mn steels. Metall and Mat Trans A 2000;31:511–30 https://doi.org/10.1007/s11661-000-0287-8.
[33] Aranas C, Wang T, Jonas JJ. Effect of interpass time on the dynamic transformation of a plain C-Mn and Nb-microalloyed steel. ISIJ Int 2015;5:647–54 https://doi.org/10.2355/isijinternational.55.647.
[34] Jonas JJ, Ghosh C, Basabe VV. Effect of dynamic transformation on the mean flow stress. Steel Res Int 2013;84:253–8 https://doi.org/10.1002/srin.201200166.
[35] Basabe VV, Jonas JJ, Ghosh C. Formation of Widmanstatten ferrite in a 0.036% Nb low carbon steel at temperatures above the Ae_3. Steel Res Int 2014;85(1):8–15 https://doi.org/10.1002/srin.201200226.
[36] Aranas C, Nguyen-Minh T, Grewal R, Jonas JJ. Flow softening-based formation of Widmanstatten ferrite in a 0.06%C steel deformed above the Ae_3. ISIJ Int 2015;55:300–7 https://doi.org/10.2355/isijinternational.55.300.
[37] Jonas JJ, He Y, Langelaan G. The rotation axes and angles involved in the formation of self-accommodating plates of Widmanstatten ferrite. Acta Matter 2014;72:13–21 https://doi.org/10.1016/j.actamat.2014.03.059.